Volume 1 | Number 1 | Jan 2013 | Pages 1–100

ChemComm

Chemical Communications
www.rsc.org/chemcomm

ROYAL SOCIETY OF CHEMISTRY

ROYAL SOCIETY OF CHEMISTRY

www.rsc.org/chemcomm

ChemComm

COMMUNICATION

Dynamics of Caged Imidazolium Cation – Toward Understanding The Order-Disorder Phase Transition and Switchable Dielectric Constant†

Xi Zhang,[a] Xiu-Dan Shao,[b] Si-Chao Li,[b] Ying Cai,[b] Ye-Feng Yao,*[a] Ren-Gen Xiong[b] and Wen Zhang*[b]
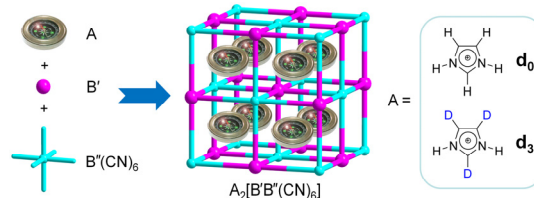
A molecular compass-like behaviour is found in a perovskite-type cage compound $(HIm)_2[KCo(CN)_6]$ (HIm = imidazolium cation). The dynamic changes of the HIm cation from static to rotating state, along with the rearrangement of host cage result in a switchable and anisotropic dielectric constant.

Crystalline compounds that consist of both rigid and motional components in the crystal lattices have recently attracted much attention, such as crystalline rotors,[1-9] dynamic porous frameworks[10-15] and molecular dielectrics and ferroelectrics.[16-21] Motional changes of polar components can arouse controlled optical and electrical properties under external stimuli.[4-6,18-21] For example, switchable dielectric constant can be realized by the transition of the polar groups between static/ordered and dynamic/disordered phases, resulting in a switching between low and high dielectric states.[21] However, this type of transition is difficult to predict and design for crystalline compounds because it depends on complicated interactions among the molecules during crystallization. As is often the cases in crystallization, well designed molecular rotors fall into a totally tight packing in crystal, which prohibits any possible internal motions under measuring conditions. Fortunately, metal-organic frameworks and inclusion compounds afford a promising means to partly overcome this serendipity of crystallization.[10,22] By exploiting the knowledge of coordination chemistry and crystal engineering, a bottom-up self-assembly approach can be used to construct various host/framework structures as shown in Scheme 1.[23] Generally, the host is rigid or static as stator while the residing guest acts as rotator. The motion is strictly confined in and modulated by the local environment of the pore. Rotations of the guests are apparently analogous to the real molecular rotators which are covalently bonded with the stator parts.

We here report a switchable dielectric compound $(HIm)_2[KCo(CN)_6]$ (HIm = imidazolium cation, **1-d$_0$**). It has a double perovskite-type structure, featured by anionic $[Co_4K_4(CN)_{12}]$ cage in which a cationic HIm guest resides. The compound exhibits two phase transitions at 198 K and 112 K, respectively, leading to stable high and low dielectric states. Compared with the analogous compound $(HIm)_2[KFe(CN)_6]$,[21a] the utilization of the diamagnetic Co(III) ion makes it possible to study the dynamics of the caged HIm cations by solid state NMR. Through combined use of single-crystal X-ray crystallography and NMR, the dynamic changes of the caged HIm cations from static to rotating state, along with the rearrangement of host cage have been revealed in great detail, providing a molecular mechanism of the transition between the high and low dielectric states of the material.


Scheme 1. General procedure of the self-assembly of subcomponents into three-dimensional packed cages: A, cationic guest (e.g. imidazolium and its deuterated analogues), showing a molecular compass-like behavior; B', monovalent metal ion; B", trivalent metal ion.
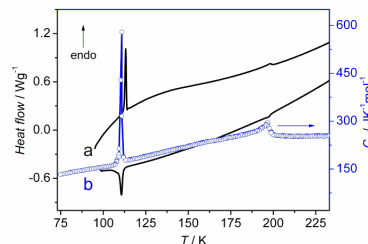
Figure 1. Thermal measurements of 1-d$_0$: (a) DSC curves and (b) heat capacity.

The two solid-state phase transitions of **1-d$_0$** were firstly disclosed by thermal analyses including DSC and C_P tests (Fig. 1). The DSC curves measured in a cooling-heating cycle show two pairs of reversible peaks, i.e., a pair of sharp ones centered around 112 K (T_1) and a pair of round peaks or steps centered around 198 K (T_2). The phase below T_1 is thus labelled as low-temperature phase (LTP) and the phases between T_1 and T_2 and above T_2 as intermediate-temperature phase (ITP) and high-temperature phase (HTP), respectively. The two sequential phase transitions were further identified by the heat capacity C_P measurement, showing a sharp λ-like peak at T_1 and a cusp at T_2.
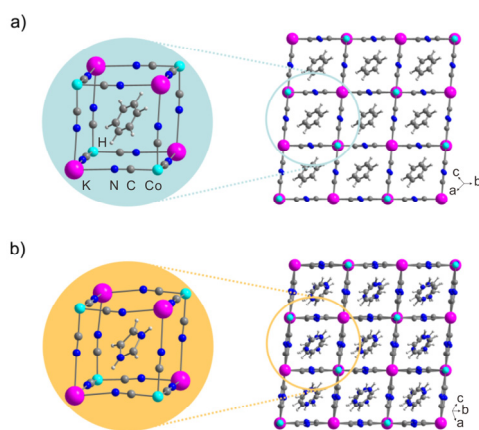
Figure 2. Crystal structures of 1-d$_0$ in the (a) HTP (293 K) and (b) LTP (93 K). In the HTP, the two nitrogen atoms of the HIm cation are refined as carbon atoms.

Crystal structure of **1-d$_0$** was measured in the temperature range 93−293 K. The basic structure unit is the [Co$_4$K$_4$(CN$_{12}$)] cage in which an HIm cation resides (Fig. 2). In the HTP and ITP, **1-d$_0$** has a centrosymmetric space group $R−3m$ while in the LTP, the space group changes to $C2/c$. This difference is reflected in the geometries of the host cage and the guest. At 293 K, the edge (Co···K) and angle (∠KCoK or ∠CoKCo) of the cage are 5.946 Å and 85.75°, respectively. In the edge of Co−C≡N···K, the N···K distance is 2.902 Å and the ∠KNC is 177.67°, indicating an almost straight line. Located at the center of the cage, the plane of the HIm guest is perpendicular to the body diagonal of the cage and also to the c axis. A highly disorder of the cation is revealed by the hexagon which is refined by modelling the atoms on the five-numbered heterocyclic HIm cation distributed over six sites as required by the crystal symmetry. The edge of the hexagon is 1.070 Å. At 93 K, either the cage or the cation guest takes striking changes with the disappearance of the threefold axis. The edges of the cage are in the range 5.903−5.940 Å, getting a little shorter, and the angles of ∠KCoK or ∠CoKCo still keep the values around 85°. Although the N···K distances of the edge change little (2.877−2.898 Å), the angles of ∠KNC obviously deviate from 180° with values in the range 169.15−170.82°. These data show the displacement of the K ions and cyanide groups, i.e., ionic nature of the N···K bond, is the main reason of the contraction of the crystal lattice that makes the structural transformation possible. As a result, the HIm guest becomes ordered in the LTP with definitely distinguishable carbon and nitrogen atoms on the five-numbered HIm ring. However, their relatively large max/min ratios of the anisotropic displacement parameters indicate the existence of a certain degree of static disorder. As a contrast, the HIm cations undergo similar disorders in the ITP and HTP. Temperature dependence of the cell parameter indicates the ITP-to-HTP transition is mainly originated from the rearrangement of the host structure (Fig. S1, ESI).

Temperature dependence of the real part (ε') of complex relative dielectric permittivity, measured along the [101] direction (HTP) of the single crystal sample of **1-d$_0$**, is shown in Figure 3 (also see Fig. S2-3, ESI). The dielectric curve exhibits two anomalies in the measured temperature range 90−280 K. One is a sharp jump at *ca.* 105 K and the other is small peak at 195 K, corresponding well to the thermal measurements (the small discrepancy arising from different rates of change of temperature). Below 105 K (LTP), the permittivity keeps nearly constant of *ca.* 6 as the low dielectric state while between 105 K and 195 K (ITP), the permittivity varies in a small degree with the values between 20−24 as the high dielectric

state. Above 195 K, the dielectric permittivity gradually decreases with the increase of the temperature due to the competition between thermal disordering and electric ordering like in polar liquids. A thermal hysteresis of *ca.* 5 K was found during the transition between LTP and ITP, reflecting very weak interactions between the cationic guests and the host lattice.
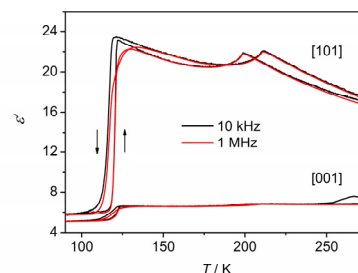
Figure 3. Temperature-dependent dielectric constants (ε') of **1-d$_0$** along the [101] and [001] directions measured at 10 kHz and 1 MHz.

A strong crystal axis-dependence of the dielectric permittivities of **1-d$_0$** is found. Large anomalies are observed in the directions perpendicular to the threefold axis (e.g. [101]) of the crystal lattice while little anomaly is recorded in the whole temperature range in the direction of threefold axis (i.e. [001]), confirming that the dielectric anisotropic properties are confined to the plane perpendicular to the threefold axis of the HTP. Such a phenomenon is consistent with the crystal structure in which the HIm cations lies in the plane perpendicular to the c axis in the HTP and can only rotate around this axis in the Co−CN−K cage. The dielectric behavior of the inclusion compound looks like a two-dimensional liquid of polar molecules.

In order to have a better understanding of the dielectric behaviour of **1-d$_0$** in molecular level, molecular dynamics of the HIm cations in the cages was investigated by wide-line ^{2}H NMR. This method can determine the geometry and frequency of rotational motions on a time-scale ranging from 10^{-4} s to 10^{-8} s.[3,24] Partially deuterated sample **1-d$_3$** was selected for the study (Fig. 1) which shows similar properties to **1-d$_0$** (Fig. S4, ESI). The experimental ^{2}H NMR spectra of **1-d$_3$** display marked changes over a large temperature range (Fig. 4). The different ^{2}H NMR line shapes in the spectra indicate that the HIm cation in the cage exhibits different reorientation processes at different temperatures. By simulating the patterns, detailed information of the reorientation processes has been obtained (More details can be found in Supporting Information).

- **The 1st transition (Fig. 4a).** Below the 1st transition temperature (e.g., 80 K), the Pake pattern spans ca. 290 kHz in width, indicating that the HIm cations are absent of motion. When the temperature is just above the 1st transition temperature (e.g., 120 K), the width of the Pake pattern is reduced by half, indicating that the HIm cations perform an axial rotation about the C$_n$ axis perpendicular to the HIm ring plane (see Model I).

- **Between the 1st and 2nd transition (Fig. 4b).** At the temperatures above the 1st transition temperature but below the 2nd transition temperature, the patterns gradually change the line shape, but the distance between the two singularities of the patterns remains unchanged. This change in the line shape was simulated with a model that considers an increase of the rotational frequency, k, of the HIm, while keeping the rotational axis unchanged. The simulated patterns match well with the experimental ones. The Arrhenius plot, k = k$_0$ exp(-Ea/RT), yields an activation energy Ea = 11.0 kJ/mol and a preexponential factor k$_0$ = 1.98*10^{11} s^{-1}.

COMMUNICATION

- **The 2nd transition (Fig. 4c).** Above the 2nd transition temperature, the pattern exhibits the characteristic motionally averaged line shape, indicating that the rotation of HIm ring has reached the fast limit. Reflecting the fast dynamics of the HIm rings, the Pake patterns of N-CD-N and N-CD-CD-N are resolved in the spectra (Fig. S6, S8, ESI). With increasing temperature the singularities at the top of both patterns exhibit a tendency to merge gradually. This change can be attributed to the out-plane oscillatory fluctuation of the HIm ring in addition to the C_n rotation (Model II).[24d] The simulation was performed based on this model. The experimental data in Fig. 4c were matched well with the simulated spectra with the fluctuation angle having a width of σ ranging from 2° at 190 K to 24° at 340 K (see Fig. S6-7, ESI).
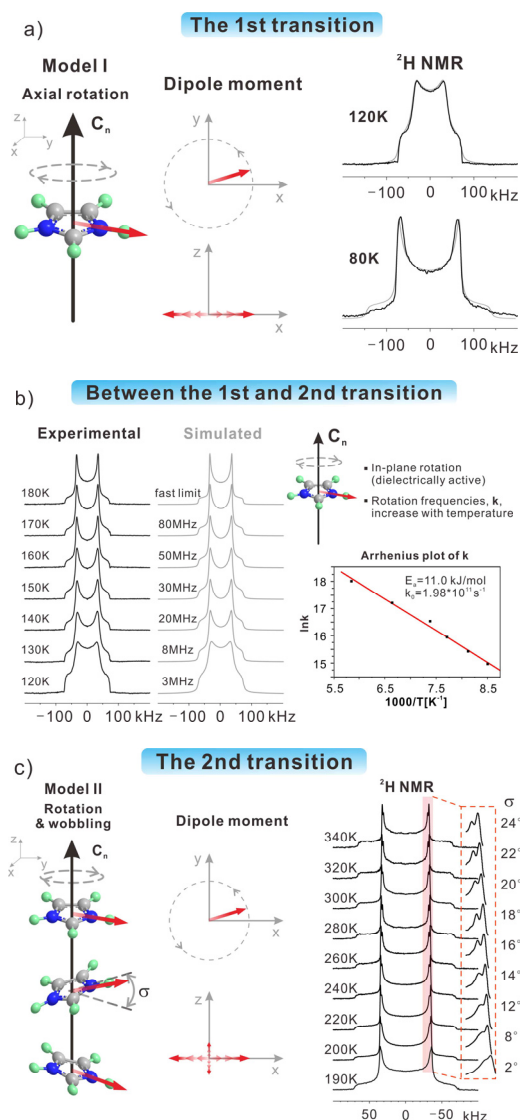
Figure 4. Simulated and experimental ^{2}H NMR spectra of 1-d$_3$: a) at 80 K and 120 K; b) from 120 K to 180 K; c) from 190 K to 340 K. The cartoon pictures in Figure 4a, b, c illustrate the motion modes of HIm cations in the cage and the induced dipole moment. In the Arrhenius plot in Fig. 4b, the rotational frequencies, k, were obtained from the ^{2}H pattern simulation. The ^{2}H patterns were simulated via the weblab (http://weblab.mpip-mainz.mpg.de/weblab/).[24c,d] In Figure 4a and b, the grey patterns were simulated based on Model I. In Figure 4c, the width of the fluctuation angle, σ, were obtained from the simulation based on Model II. More details about the simulation can be found in Supporting Information (Fig. S5-7, ESI).

The temperature-dependent motions of the HIm revealed by the above ^{2}H NMR provide us a deep understanding of the dielectric responses of the material at the different temperatures. At the 1st transition, the HIm ring in the cage starts to perform the in-plane rotation about the Cn axis. The rotation of HIm ring can induce a rotation of the dipole moment in the [001] plane (see the cartoon picture in Fig. 4a) and thus the sudden change of the dielectric permittivity. If considering the rotation of the dipolar moment of HIm as the only contribution to the change of the dielectric permittivity, $\Delta\varepsilon'$, the rotational geometry of the HIm ring indicates that the maximum $\Delta\varepsilon'$ should appear in the [100] or [010] plane, i.e., perpendicular to the HIm ring plane (here a naturally grown plane [101] was measured instead), and the minimum $\Delta\varepsilon'$ should appear on the [001] plane that is parallel to the HIm ring. This derivation is well consistent with the observation in the dielectric measurement shown in Fig. 3.

Between the 1st and 2nd transition, the HIm rings still perform the in-plane rotation and thus the high dielectric state of the material is maintained. The gradual decrease of the dielectric permittivity at this temperature range can be related to the thermal motion against the alignment of the molecular dipole moments in the electric field direction as revealed by Debye equation.

At the 2nd transition, the HIm rings start the out-plane oscillatory fluctuation in addition to the C_n rotation. This increase in freedom of the molecular motion reflects the expansion of the host structure in HTP, and thus is in line with the X-ray observation. The out-plane oscillatory fluctuation of HIm rings is considered to have a direct relation to the 2nd transition of the dielectric permittivity. But the contribution of this motion to the dielectric permittivity of the sample is twofold. Firstly, it is straightforward that the oscillatory fluctuation changes the orientation of the dipole moment of HIm cation and thus is dielectrically active (see the cartoon picture in Fig. 4c). Secondly, it has been noticed that in a cage in HTP the centre of the equivalent negative charge does not completely overlap with the centre of the positive charge of the HIm ring (Fig. S9, ESI). A dipole moment between the positive charge and the equivalent negative charge thus exists. When the HIm ring starts the fluctuation, the dipole moment most likely fluctuates too. This may induce an additional dielectric response that contributes to the 2nd transition of the dielectric permittivity.

Conclusions

We report a perovskite-type cage compound (HIm)$_2$[KCo(CN)$_6$] (**1-d$_0$**, HIm = imidazolium cation) showing a molecular compass-like behavior. The guest HIm cation resides in the anionic host Co$_4$K$_4$(CN)$_{12}$ cage and undergoes dynamic changes from static to rotating state. The order-disorder mechanism, along with the host rearrangement, is responsible for the transition between the low and high dielectric state. Compound **1-d$_0$** presents a new class of crystalline molecular rotary dielectrics that shows striking dielectric anomaly and anisotropy. Investigations on such systems shed light on the search for new electric ordering materials based on molecular materials and understanding of the motions of dipole moments in crystal lattices.

Acknowledgements

Notes and references

[a] Address here. X. Zhang, Prof. Y.-F. Yao
Department of Physics & Shanghai Key Laboratory of Magnetic Resonance, East China Normal University, North Zhongshan Road 3663, Shanghai 200062, China
E-mail: yfyao@phy.ecnu.edu.cn

[b] X.-D. Shao, S.-C. Li, Y. Cai, Prof. R.-G. Xiong, Prof. W. Zhang
Ordered Matter Science Research Center, Southeast University, Nanjing 211189, China
E-mail: zhangwen@seu.edu.cn

† Electronic Supplementary Information (ESI) available: DSC, dielectric measurements, ^{2}H NMR spectra, Single-Crystal X-ray and crystallographic structure. CCDC 1012553−1012555 or other electronic format see DOI: 10.1039/ c000000x/

1 C. S. Vogelsberg, M. A. Garcia-Garibay, *Chem. Soc. Rev.* 2012, **41**, 1892-1910.

2 (a) G. S. Kottas, L. I. Clarke, D. Horinek and J. Michl, *Chem. Rev.* 2005, **105**, 1281-1376; (b) J. Michl, E. C. H. Sykes, *ACS NANO* 2009, **3**, 1042-1048.

3 S. D. Karlen, H. Reyes, R. E. Taylor, S. I. Khan, M. F. Hawthorne and M. A. Garcia-Garibay, *Proc. Natl. Acad. Sci. U.S.A.* 2010, **107**, 14973-14977.

4 (a) C. Lemouchi, C. S. Vogelsberg, L. Zorina, S. Simonov, P. Batail, S. Brown and M. A. Garcia-Garibay, *J. Am. Chem. Soc.* 2011, **133**, 6371-6379; (b) C. Lemouchi, K. Iliopoulos, L. Zorina, S. Simonov, P. Wzietek, T. Cauchy, A. Rodríguez-Fortea, E. Canadell, J. Kaleta, J. Mi chl, D. Gindre, M. Chrysos and P. Batail, *J. Am. Chem. Soc.* 2013, **135**, 9366-9376.

5 (a) W. Setaka, K. Yamaguchi, *J. Am. Chem. Soc.* 2012, **134**, 12458-12461; (b) W. Setaka, K. Yamaguchi, *Proc. Natl. Acad. Sci. U.S.A.* 2012, **109**, 9271-9275; (c) W. Setaka, K. Yamaguchi, *J. Am. Chem. Soc.* 2013, **135**, 14560-14563.

6 (a) M. Horie, T. Sassa, D. Hashizume, Y. Suzaki, K. Osakada and T. Wada, *Angew. Chem. Int. Ed.* 2007, **46**, 4983-4986; (b) M. Horie, Y. Suzaki, D. Hashizume, T. Abe, T. Wu, T. Sassa, T. Hosokai and K. Osakada, *J. Am. Chem. Soc.* 2012, **134**, 17932-17944.

7 (a) H. Deng, M. A. Olson, J. F. Stoddart and O. M. Yaghi, *Nat. Chem.* 2010, **2**, 439-443; (b) V. N. Vukotic, K. J. Harris, K. Zhu, R. W. Schurko, S. J. Loeb, *Nat. Chem.* 2012, **4**, 456-460.

8 A. N. Sokolov, D. C. Swenson and L. R. MacGillivray, *Proc. Natl. Acad. Sci. U.S.A.* 2008, **105**, 1794-1797.

9 Q.-C. Zhang, F.-T. Wu, H.-M. Hao, H. Xu, H.-X. Zhao, L.-S. Long, R.-B. Huang and L.-S. Zheng, *Angew. Chem. Int. Ed.* 2013, **52**, 12602-12605.

10 (a) S. Kitagawa, R. Kitaura and S.-i. Noro, *Angew. Chem. Int. Ed.* 2004, **43**, 2334-2375; (b) J. J. Vittal, *Coord. Chem. Rev.* 2007, **251**, 1781-1795; (c) S. Horike, S. Shimomura and S. Kitagawa, *Nat. Chem.* 2009, **1**, 695-704; d) E. Coronado, G. Minguez Espallargas, *Chem. Soc. Rev.* 2013, **42**, 1525-1539.

11 S. Horike, R. Matsuda, D. Tanaka, S. Matsubara, M. Mizuno, K. Endo and S. Kitagawa, *Angew. Chem. Int. Ed.* 2006, **45**, 7226-7230.

12 (a) J. A. Rodríguez-Velamazán, M. A. González, J. A. Real, M. Castro, M. C. Muñoz, A. B. Gaspar, R. Ohtani, M. Ohba, K. Yoneda, Y. Hijikata, N. Yanai, M. Mizuno, H. Ando and S. Kitagawa, *J. Am. Chem. Soc.* 2012, **134**, 5083-5089; (b) E. Coronado, M. Giménez-Marqués, G. Mínguez Espallargas, F. Rey and I. J. Vitórica-Yrezábal, *J. Am. Chem. Soc.* 2013, **135**, 15986-15989.

13 N. B. Shustova, T.-C. Ong, A. F. Cozzolino, V. K. Michaelis, R. G. Griffin and M. Dincă, *J. Am. Chem. Soc.* 2012, **134**, 15061-15070.

14 C. R. Murdock, N. W. McNutt, D. J. Keffer and D. M. Jenkins, *J. Am. Chem. Soc.* 2014, **136**, 671-678.

15 (a) A. Comotti, S. Bracco, A. Yamamoto, M. Beretta, T. Hirukawa, N. Tohnai, M. Miyata and P. Sozzani, *J. Am. Chem. Soc.* 2014, **136**, 618-621; (b) A. Comotti, S. Bracco, T. Ben and S. Qiu, P. Sozzani, *Angew. Chem. Int. Ed.* 2014, **53**, 1043-1047.

16 (a) F. Jona, G. Shirane, *Ferroelectric Crystals* and Pergamon Press: New York, 1962; (b) M. E. Lines, A. M. Glass, *Principles and Applications of Ferroelectrics and Related Materials*, Oxford University Press: Oxford, U.K., 1991; (c) Z. G. E. Ye, Woodhead Publishing: Cambridge, U.K., 2008.

17 (a)S. Horiuchi, Y. Tokura, *Nat. Mater.* 2008, **7**, 357-366; (b) W. Zhang, R.-G. Xiong, *Chem. Rev.* 2012, **112**, 1163-1195.

18 (a) T. Akutagawa, H. Koshinaka, D. Sato, S. Takeda, S.-I. Noro, H. Takahashi, R. Kumai, Y. Tokura and T. Nakamura, *Nat. Mater.* 2009, **8**, 342-347; (b) D.-W. Fu, W. Zhang, H.-L. Cai, Y. Zhang, J.-Z. Ge, R.-G. Xiong and S. D. Huang, *J. Am. Chem. Soc.* 2011, **133**, 12780-12786; (c) D.-W. Fu, H.-L. Cai, S.-H. Li, Q. Ye, L. Zhou, W. Zhang, Y. Zhang, F. Deng and R.-G. Xiong, *Phys. Rev. Lett.* 2013, **110**, 257601.

19 (a) P. Jain, N. S. Dalal, B. H. Toby, H. W. Kroto and A. K. Cheetham, *J. Am. Chem. Soc.* 2008, **130**, 10450-10451; (b) P. Jain, V. Ramachandran, R. J. Clark, H. D. Zhou, B. H. Toby, N. S. Dalal, H. W. Kroto and A. K. Cheetham, *J. Am. Chem. Soc.* 2009, **131**, 13625-13627; (c) D.-W. Fu, W. Zhang, H.-L. Cai, Y. Zhang, J.-Z. Ge, R.-G. Xiong, S. D. Huang and T. Nakamura, *Angew. Chem. Int. Ed.* 2011, **50**, 11947-11951; (e) Z.-H. Sun, J.-H. Luo, T.-L. Chen, L.-N. Li, R.-G. Xiong, M.-L. Tong and M.-C. Hong, *Adv. Funct. Mater.* 2012, **22**, 14855-4861; (f) C.-M. Ji, Z.-H. Sun, S.-Q. Zhang, T.-L. Chen, P. Zhou and J.-H. Luo, *J. Mater. Chem. C* 2014, **2**, 567-572.

20 Y. Zhang, W. Zhang, S.-H. Li, Q. Ye, H.-L. Cai, F. Deng, R.-G. Xiong and S. D. Huang, *J. Am. Chem. Soc.* 2012, **134**, 11044-11049.

21 (a) W. Zhang, Y. Cai, R.-G. Xiong, H. Yoshikawa and K. Awaga, *Chem. Int. Ed.* 2010, **49**, 6608-6610; (b) W. Zhang, H.-Y. Ye, R. Graf, H. W. Spiess, Y.-F. Yao, R.-Q. Zhu and R.-G. Xiong, *J. Am. Chem. Soc.* 2013, **135**, 5230-5233.

22 J. L. Atwood, J. E. D. Davies and D. D. MacNicol, (Eds.) *Inclusion Compounds*, Academic Press: UK, 1984.

23 (a) C. B. Aakeroy, K. R. Seddon, *Chem. Soc. Rev.* 1993, **22**, 397-407; (b) G. A. Jeffrey, *An Introduction to Hydrogen Bonding*, Oxford University Press: USA, 1997; (c) D. Braga, F. Grepioni and G. R. Desiraju, *Chemical Reviews* 1998, **98**, 1375-1406; (d) J. W. Steed, *Supramolecular Chemistry*, John Wiley & Sons: West Sussex, U.K., 2000.

24 (a) H. W. Spiess, *NMR basic principles and progress, Vol. 15*, Springer-Verlag, Berlin, 1978; (b) K. Schmidt-Rohr, H. W. Spiess, *Multidimensional Solid-State NMR and Polymers*, Academic Press, London, 1994; (c) V. Macho, L. Brombacher and H. W. Spiess, *Appl. Magn. Reson.* 2001, **20**, 405-432; (d) M. R. Hansen, R. Graf and H. W. Spiess. *Acc. Chem. Res.* 2012, **46**, 1996-2007.